Wireless Pers Commun (2015) 82:1733–1747
DOI 10.1007/s11277-015-2309-2

Performance Analysis of Full-Rate Coordinate Interleaved Orthogonal Designs Over Time-Selective Fading Channels

Van-Bien Pham

Published online: 28 January 2015

Abstract Coordinate interleaved orthogonal designs (CIOD) (Khan and Rajan in IEEE Trans Inform Theory 52(5):2062–2091, 2006) can offer desirable properties, such as full rate, full diversity and single-symbol maximum likelihood decoding for two, three and four transmit antennas under quasi-static fading channels. When fading is time-selective, zero-forcing decoder can applied to achieve good performance while still maintain low decoding complexity. In this paper, theoretical analysis of symbol error rate performance for CIOD codes over time-selective fading channels with a zero-forcing linear receiver is derived. Firstly, a closed-form expression (i.e., not in integral form) is derived for the average symbol pair-wise error probability (SPEP) in time-selective frequency-nonselective independent identically distributed (i.i.d.) Rayleigh fading channels. Then, the SPEP is used to derive a tight upper bound (UB) for the symbol-error rate (SER) of CIOD codes. Simulation results indicate that our theoretical UB often coincides (within 0.05 dB) with the true SER obtained via Monte-Carlo simulation. The UB can thus be used to accurately predict and optimize the performance of CIOD codes over time-selective fading channels.

Keywords CIOD · ZF decoding · Performance analysis · Time-selective fading

1 Introduction

Space-Time Coding is an effective approach to achieve transmit diversity in multiple-input multiple-output (MIMO) systems [1]. Orthogonal space-time block codes (OSTBCs) [2, 3] attain full diversity and optimum performance with single-symbol maximum likelihood decoder (SSD), but they suffer a rate loss when there have more than two transmit antennas. The rate of OSTBCs is 1 spcu (symbol per channel use) for two transmit antennas and 3/4 for three and four transmit antennas. Quasi-orthogonal SBTCs (QOSTBCs) [4–6] and QOSTBCs with constellation rotation (CR-QOSTBCs) [7,8] have a rate of one for three

V.-B. Pham (✉)
Faculty of Radio Electronic, Le Quy Don Technical University, Hanoi, Vietnam
e-mail: phamvanbien@mta.edu.vn

and four transmit antennas, but they require a high complexity pair-wise symbol maximum likelihood decoder (PSD). To eliminate the drawback of QOSTBCs and CR-QOSTBCs, Khan et al. [9,10] proposed CIOD codes which achieve full rate and full diversity for three and four transmit antennas with SSD decoder.

Decoding and performance analysis of CIOD codes were performed in many previous researches [11,12]. However, these researches only focus on quasi-static fading channels, assuming that the channel is static within codeword duration and varies independently from one codeword to another; but this assumption is not always true in practice. In fact, the time-selective fading channel model exists due to Doppler shifts and carrier frequency offsets. For example, the 3G European cellular standard is required to operate on trains moving up to 500 km/h, which can induce Doppler shifts of up to 800 Hz for a carrier frequency of 2 GHz [13]. In such a communications scenario, the channel may vary significantly from symbol to symbol. In the time-selective channel model, the SSD decoding of CIOD codes previously proposed in [10] and [11] no longer offers optimum performance, which can lead to error floor at high SNR values. To avoid exhibiting error floors, Lee et al. [13] propose a simple ZF linear decoder where inter-symbol interference (ISI) was completely removed. However, what this research fails to accomplish is deriving the closed-form analytical expressions for error performance.

This paper provides theoretical analysis of symbol-error rate (SER) performance of CIOD codes when a ZF decoder is used. We firstly derive the closed-form analytical expression (i.e., not in integral form) for the symbol pair-wise error probability (SPEP). We then use the SPEP to derive a union bound (UB) on SER for CIOD codes. Extensive simulation results show that the UB is within 0.05 dB from the simulated SER when SER $< 10^{-2}$. Moreover, our theoretical performance analysis is general and can be applied for an arbitrary input signal constellation and an arbitrary number of receiver antennas. The UB can thus be used to accurately predict and optimize the performance of CIOD codes over time-selective fading channels, where quasi-static flat fading channel is considered as a special case.

The rest of this paper is organized as follows. The channel model and ZF decoding are presented in Sect. 2. Performance analysis and union bound on SER are presented in Sect. 3. Simulation results are given in Sect. 4. Section 5 concludes the paper.

We use the following notations throughout this letter. The superscripts $(\cdot)^{\mathrm{T}}$ denotes transpose operations. $\Pr(\cdot)$ denotes the probability. $E[\cdot]$ is reserved for expectation with respect to all the random variables within the braces. $x \sim \mathcal{CN}(m, \sigma^2)$ stands for circular symmetric complex Gaussian variable x with mean m and variance σ^2. $\mathrm{j} = \sqrt{-1}$.

2 Channel Model and ZF Decoding

2.1 Channel Model

Consider an uncorrelated MIMO system with N_T transmit antennas (Tx) and N_R received antennas (Rx). A STBC encodes an input symbol vector of length $K, \boldsymbol{s} = [s_1\, s_2 \ldots s_K]^{\mathrm{T}}$ into an $L \times N_R$ matrix $\boldsymbol{S}$, where L is the number of time slots. Symbol rate of the STBC $\boldsymbol{S}$ is K/L. If $K = L$, then $\boldsymbol{S}$ is called full-rate code. The received signal $r_m(t)$ on mth receive antenna at tth time slot is given by

$$r_m(t) = \sum_{i=1}^{N_T} h_{im}(t) z_{ti} + n_m(t) \tag{1}$$

where $h_{im}(t)$ and $n_m(t)$ denote path gain from ith transmit antenna to mth receive antenna and noise on mth receive antenna at tth time slot, respectively. z_{ti} denotes transmitted signal on ith transmit antenna at tth time slot. In this paper, we make the following assumptions about the channel model (1): $n_m(t)$ is a identically distributed zero-mean circularly symmetric complex Gaussian random variable satisfying $E[n_m(t_1)n_m^*(t_2)] = \begin{cases} N_0; & \text{if } t_1 = t_2 \text{ and } k = m \\ 0; & \text{othewise} \end{cases}$; $h_{im}(t),\ i = 1, \ldots,\ N_T,\ m = 1, \ldots, N_R$ is i.d.d random variables with zero-mean and unit-variance satisfying $E\left[|h_{im}(t)|^2\right] = 1$; sufficient antenna spacing, so that $E\left[h_{im}(\cdot)h_{kn}^*(\cdot)\right] = 0$ if $i \neq k$ and/or $m \neq n$; relaxing this constraint would be possible, but it would complicate the analysis and it would detract from our main aim of studying the impact of time variations; temporally symmetric Rayleigh fading, so that the correlation $\rho(m)$ between $h_{im}(t)$ and $h_{in}(t+n)$ is the same for $\forall i = 1, \ldots, N_T$, $\forall m = 1, \ldots, N_R$ namely $E\left[h_{im}(t)h_{im}^*(t+n)\right] = \rho(n) \forall i, m$; perfect knowledge of $h_{im}(t) (i = 1, .., N_T,\ m = 1, \ldots,\ N_R$, and $t = 1, .., L)$ at the receiver. According to Jakes' model [14], we have $\rho(n) = J_0(2\pi n f_d T_s)$ where $J_0(\cdot)$ is the zero-order Bessel function of the first kind, f_d is the maximum Doppler shift and T_s is the period of each symbol. If $f_d T_s = 0$ we obtain quasi-static fading channel model; otherwise we obtain time-selective fading channel model.

In [9,10], the codeword matrix of full rate CIODs $\boldsymbol{S}_2, \boldsymbol{S}_3, \boldsymbol{S}_4$ for $\mathrm{N_T} = 2, 3, 4$ given as following:

$$\boldsymbol{S}_2 = \begin{bmatrix} z_1 & 0 \\ 0 & z_2 \end{bmatrix}; \boldsymbol{S}_3 = \begin{bmatrix} z_1 & z_2 & 0 \\ -z_2^* & z_1^* & 0 \\ 0 & 0 & z_3 \\ 0 & 0 & -z_4^* \end{bmatrix}; \boldsymbol{S}_4 = \begin{bmatrix} z_1 & z_2 & 0 & 0 \\ -z_2^* & z_1^* & 0 & 0 \\ 0 & 0 & z_3 & z_4 \\ 0 & 0 & -z_4^* & z_3^* \end{bmatrix} \tag{2}$$

where the transmitted complex symbols z_i are generated by coordinate interleaving as $z_i = s_{iI} + \mathrm{j}s_{(i+K/2)Q}$ when $i = 1, \ldots,\ K/2$, and $z_i = s_{iI} + \mathrm{j}s_{(i-K/2)Q}$ when $i = 1 + K/2, \ldots, K$.

We consider CIOD code with $N_\mathrm{T} = 4$ given in (2). After some straightforward manipulations of (1), the input-output relationship of the CIOD code can be expressed in vector/matrix form as

$$\boldsymbol{r} = \boldsymbol{\mathcal{H}}\mathbf{z} + \boldsymbol{n} \tag{3}$$

where $\boldsymbol{r}$ is the $4N_R \times 1$ received signal vector, $\mathbf{z} = (z_1,\ z_2,\ z_3,\ z_4)^\mathrm{T}$ is the 4×1 transmitted signal vector, $\boldsymbol{n}$ is the $4N_\mathrm{R} \times 1$ AWGN noise vector, and $\boldsymbol{\mathcal{H}} = \left[\boldsymbol{H}_1\ \boldsymbol{H}_2 \cdots \boldsymbol{H}_{N_R}\right]^\mathrm{T}$ is the effective channel matrix whose submatrix $\boldsymbol{H}_m,\ m = 1, ..., N_\mathrm{R}$ for CIOD code with $N_\mathrm{T} = 4$ is given by

$$\boldsymbol{H}_m(\boldsymbol{S}_4) = \begin{bmatrix} h_{1m}(1) & h_{2m}(1) & 0 & 0 \\ h_{2m}^*(2) & -h_{1m}^*(2) & 0 & 0 \\ 0 & 0 & h_{3m}(3) & h_{4m}(3) \\ 0 & 0 & h_{4m}^*(4) & -h_{3m}^*(4) \end{bmatrix} \tag{4}$$

where the index inside $(\cdot)$ is the discrete time index with respect to the symbol time duration in each codeword period.

2.2 Zero-Forcing (ZF) Decoding

Based on the decoding method presented in [15,16], which is originally for the Alamouti STBC [2] with two transmit antennas over time-selective fading channels, Lee et al. [13] propose an efficient ZF decoding method for channel model (3) is introduced as follows. First, a simple matrix transformation for orthogonal combining is introduced as

$$\bar{\boldsymbol{A}} = \begin{bmatrix} -a_{22} & a_{12} \\ a_{21} & -a_{11} \end{bmatrix} \text{for} \quad \boldsymbol{A} = \begin{bmatrix} a_{11} & a_{12} \\ a_{21} & a_{22} \end{bmatrix} \tag{5}$$

Then, by combining $\boldsymbol{r}$ in (3) by $\bar{\boldsymbol{\mathcal{H}}} = \left[\bar{\boldsymbol{H}}_1, \bar{\boldsymbol{H}}_2, \ldots, \bar{\boldsymbol{H}}_{N_R}\right]$ with the submatrices

$$\bar{\boldsymbol{H}}_m = \begin{bmatrix} h_{1m}^*(2) & h_{2m}(1) & 0 & 0 \\ h_{2m}^*(2) & -h_{1m}(1) & 0 & 0 \\ 0 & 0 & h_{3m}^*(4) & h_{4m}(3) \\ 0 & 0 & h_{4m}^*(4) & -h_{3m}(3) \end{bmatrix}; m = 1, 2, ..., N_R \tag{6}$$

obtain

$$\underbrace{\bar{\boldsymbol{\mathcal{H}}}\boldsymbol{r}}_{\bar{\boldsymbol{y}}} = \underbrace{\bar{\boldsymbol{\mathcal{H}}}\boldsymbol{\mathcal{H}}}_{\bar{\boldsymbol{G}}}\boldsymbol{s} + \underbrace{\bar{\boldsymbol{\mathcal{H}}}\boldsymbol{n}}_{\bar{\boldsymbol{n}}} \tag{7}$$

$$\Rightarrow \begin{bmatrix} \bar{y}(1) \\ \bar{y}(2) \\ \bar{y}(3) \\ \bar{y}(4) \end{bmatrix} = \begin{bmatrix} g_1 & 0 & 0 & 0 \\ 0 & g_1 & 0 & 0 \\ 0 & 0 & g_2 & 0 \\ 0 & 0 & 0 & g_2 \end{bmatrix} \begin{bmatrix} z_1 \\ z_2 \\ z_3 \\ z_4 \end{bmatrix} + \begin{bmatrix} \bar{n}(1) \\ \bar{n}(2) \\ \bar{n}(3) \\ \bar{n}(4) \end{bmatrix} \tag{8}$$

where

$$\begin{aligned} g_1 &= \sum\nolimits_{k=1}^{N_R} \left(h_{1k}^*(2)h_{1k}(1) + h_{2k}^*(2)h_{2k}(1)\right); \\ g_2 &= \sum\nolimits_{k=1}^{N_R} \left(h_{3k}^*(4)h_{3k}(3) + h_{4k}^*(4)h_{4k}(3)\right) \end{aligned} \tag{9}$$

By multiplying both sides in Eq. (8) by $\bar{\boldsymbol{G}}^{\mathrm{H}}$ we obtain

$$\underbrace{\bar{\boldsymbol{G}}^{\mathrm{H}}\bar{\boldsymbol{y}}}_{\bar{\bar{\boldsymbol{y}}}} = \underbrace{\bar{\boldsymbol{G}}^{\mathrm{H}}\bar{\boldsymbol{G}}}_{\boldsymbol{D}}\boldsymbol{s} + \underbrace{\bar{\boldsymbol{G}}^{\mathrm{H}}\bar{\boldsymbol{n}}}_{\bar{\boldsymbol{v}}} \tag{10}$$

$$\Rightarrow \begin{bmatrix} \bar{\bar{y}}(1) \\ \bar{\bar{y}}(2) \\ \bar{\bar{y}}(3) \\ \bar{\bar{y}}(4) \end{bmatrix} = \begin{bmatrix} |g_1|^2 & 0 & 0 & 0 \\ 0 & |g_1|^2 & 0 & 0 \\ 0 & 0 & |g_2|^2 & 0 \\ 0 & 0 & 0 & |g_2|^2 \end{bmatrix} \begin{bmatrix} z_1 \\ z_2 \\ z_3 \\ z_4 \end{bmatrix} + \begin{bmatrix} \bar{v}(1) \\ \bar{v}(2) \\ \bar{v}(3) \\ \bar{v}(4) \end{bmatrix} \tag{11}$$

where

$$\bar{v}_1 \sim \mathcal{CN}\left(0, |g_1|^2 \lambda_1 N_0\right); \quad \bar{v}_2 \sim \mathcal{CN}\left(0, |g_1|^2 \lambda_2 N_0\right); \tag{12}$$

$$\bar{v}_3 \sim \mathcal{CN}\left(0, |g_2|^2 \lambda_3 N_0\right); \quad \bar{v}_4 \sim \mathcal{CN}\left(0, |g_2|^2 \lambda_4 N_0\right); \tag{13}$$

$$\lambda_1 = \sum\nolimits_{k=1}^{N_R} \left(|h_{1k}(2)|^2 + |h_{2k}(1)|^2\right); \quad \lambda_2 = \sum\nolimits_{k=1}^{N_R} \left(|h_{1k}(1)|^2 + |h_{2k}(2)|^2\right); \tag{14}$$

$$\lambda_3 = \sum\nolimits_{k=1}^{N_R} \left(|h_{3k}(4)|^2 + |h_{4k}(3)|^2\right); \quad \lambda_4 = \sum\nolimits_{k=1}^{N_R} \left(|h_{3k}(3)|^2 + |h_{4k}(4)|^2\right) \tag{15}$$

From (11) we can see that orthogonality can be achieved without interference terms at the cost of increasing the variance of noise terms in noise vector $\bar{\boldsymbol{v}}$. After pre-whitening noise and de-interleaving, we obtain

$$\hat{y}_1 = \frac{\bar{\bar{y}}_1}{|g_1|\sqrt{\lambda_1}} + j\frac{\bar{\bar{y}}_3}{|g_2|\sqrt{\lambda_3}} = \frac{|g_1|}{\sqrt{\lambda_1}}s_{1I} + j\frac{|g_2|}{\sqrt{\lambda_3}}s_{1Q} + v_1 \tag{16a}$$

$$\hat{y}_2 = \frac{\bar{\bar{y}}_2}{|g_1|\sqrt{\lambda_2}} + j\frac{\bar{\bar{y}}_4}{|g_2|\sqrt{\lambda_4}} = \frac{|g_1|}{\sqrt{\lambda_2}}s_{2I} + j\frac{|g_2|}{\sqrt{\lambda_4}}s_{2Q} + v_2 \tag{16b}$$

$$\hat{y}_3 = \frac{\bar{\bar{y}}_3}{|g_2|\sqrt{\lambda_3}} + j\frac{\bar{\bar{y}}_1}{|g_1|\sqrt{\lambda_1}} = \frac{|g_2|}{\sqrt{\lambda_3}}s_{3I} + j\frac{|g_1|}{\sqrt{\lambda_1}}s_{3Q} + v_3 \tag{16c}$$

$$\hat{y}_4 = \frac{\bar{\bar{y}}_4}{|g_2|\sqrt{\lambda_4}} + j\frac{\bar{\bar{y}}_2}{|g_1|\sqrt{\lambda_2}} = \frac{|g_2|}{\sqrt{\lambda_4}}s_{4I} + j\frac{|g_1|}{\sqrt{\lambda_2}}s_{4Q} + v_4 \tag{16d}$$

Finally, we obtain the following ZF decision metrics

$$\hat{s}_1 = \arg\min_{s\in\mathcal{A}e^{j\theta}} \left[\left| \hat{y}_{1I} - \frac{|g_1|}{\sqrt{\lambda_1}}s_I \right|^2 + \left| \hat{y}_{1Q} - \frac{|g_2|}{\sqrt{\lambda_3}}s_Q \right|^2 \right] \tag{17a}$$

$$\hat{s}_2 = \arg\min_{s\in\mathcal{A}e^{j\theta}} \left[\left| \hat{y}_{2I} - \frac{|g_1|}{\sqrt{\lambda_2}}s_I \right|^2 + \left| \hat{y}_{2Q} - \frac{|g_2|}{\sqrt{\lambda_4}}s_Q \right|^2 \right] \tag{17b}$$

$$\hat{s}_3 = \arg\min_{s\in\mathcal{A}e^{j\theta}} \left[\left| \hat{y}_{3I} - \frac{|g_2|}{\sqrt{\lambda_3}}s_I \right|^2 + \left| \hat{y}_{3Q} - \frac{|g_1|}{\sqrt{\lambda_1}}s_Q \right|^2 \right] \tag{17c}$$

$$\hat{s}_4 = \arg\min_{s\in\mathcal{A}e^{j\theta}} \left[\left| \hat{y}_{4I} - \frac{|g_2|}{\sqrt{\lambda_4}}s_I \right|^2 + \left| \hat{y}_{4Q} - \frac{|g_1|}{\sqrt{\lambda_2}}s_Q \right|^2 \right] \tag{17d}$$

Although v_1, v_2, v_3, and v_4 are correlated, the ZF detector ignores the correlation, and arrives at suboptimal decisions by independently quantizing $\hat{y}_1$, $\hat{y}_2$, $\hat{y}_3$ and $\hat{y}_4$. Therefore, the decoder is called a linear quasi-maximum likelihood decoder. When channel is static, then v_1, v_2, v_3, and v_4 are independent and the ZF detector achieves optimum decoding performance as does the SSD detector. We also notice that although the ZF decoder is presented for the CIOD code with $N_T = 4$ (i.e., $\boldsymbol{S}_4$), CIOD codes with $N_T = 2$ and 3 (i.e., $\boldsymbol{S}_2$ and $\boldsymbol{S}_3$) can be directly applied over time-selective fading channels.

3 Performance Analysis of CIOD Codes

We consider CIOD code with $N_T = 4$, (i.e., $\boldsymbol{S}_4$) and channel model (3). We remark that, from the symmetry of the channel model, we only need to derive the error probability for the first symbol s_1, knowing that the other symbols will have the same error probability. From (15), the SPEP conditioned on the fading coefficients can be expressed as

$$\begin{aligned} \Pr\left(s \to \hat{s} \,|\boldsymbol{H}\right) &= \Pr\left(\left| \hat{y} - \frac{|g_1|}{\sqrt{\lambda_1}}\hat{s}_I - \frac{|g_2|}{\sqrt{\lambda_3}}\hat{s}_Q \right|^2 < \left| \hat{y} - \frac{|g_1|}{\sqrt{\lambda_1}}u_I - \frac{|g_2|}{\sqrt{\lambda_3}}u_Q \right|^2 \right. \\ &\qquad \left. = \left| v_I + jv_Q \right|^2 \right) \\ &= Q\left(\sqrt{\frac{SNR}{4}\left(\frac{|g_1|^2}{\lambda_1}\Delta_I^2 + \frac{|g_2|^2}{\lambda_3}\Delta_Q^2 \right)} \right) \end{aligned} \tag{18}$$

where $s \to \hat{s}$ denotes a pair-wise error event, $\Delta_I^2 \triangleq \frac{|s_I - \hat{s}_I|^2}{E_s/2}$ and $\Delta_Q^2 \triangleq \frac{|s_Q - \hat{s}_Q|^2}{E_s/2}$ represent the normalized squared Euclidean distances along the in-phase and quadrature directions, respectively. $\hat{y}$ and v denote the received signal and noise signal, after noise pre-whitening and de-interleaving, hence $v_I, v_Q \sim \mathcal{CN}\left(0, \frac{N_0}{2}\right)$. E_s is the total transmitted power on transmit antennas per symbol duration and $SNR = E_s/N_0$ denote average signal-to-noise ratio at the receiver. Since the symbol pair-wise error event for each $s_i \to \hat{s}_i$ has an identical distribution, it suffices to consider the case of $s_1 \to \hat{s}_1$ for the evaluation, so we drop the subscript without loss of generality. Then, averaging the instantaneous SPEP given in (18) over the channel realization yields the average SPEP as follows

$$\Pr\left(s \to \hat{s}\right) = \int_0^\infty Q\left(\sqrt{\omega}\right) p_W(\omega) d\omega = \int_0^\infty \frac{1}{2}\text{erfc}\left(\sqrt{\frac{\omega}{2}}\right) p_W(\omega) d\omega \tag{19}$$

where $Q(x) = \frac{1}{\sqrt{2\pi}} \int_x^\infty \exp\left(-\frac{u^2}{2}\right) du$, $\text{erfc}(x) = \frac{2}{\sqrt{\pi}} \int_x^\infty \text{e}^{-u^2} du$, and

$$\omega = \frac{|g_1|^2}{\lambda_1} \frac{SNR}{4} \Delta_I^2 + \frac{|g_2|^2}{\lambda_3} \frac{SNR}{4} \Delta_Q^2 \tag{20}$$

To calculate average SPEP (24), we need to derive the probability density function (PDF) $p_W(\omega)$ of random variable ω (20). We give the following theorem.

Theorem 1 *For a channel model* (3) *with assumptions in* Sect. 2.1*, a random variable* ω *given in* (20) *has PDF as*

$$\begin{aligned} p_W(\omega) = & \sum_{k_1=0}^{2N_R-1} \sum_{k_2=0}^{2N_R-1} a_1 a_2 \frac{\rho^{2(k_1+k_2)} \left(1-\rho^2\right)^{4N_R-2-k_1-k_2}}{k_1! k_2! c_I^{k_1+1} c_Q^{k_2+1}} \\ & \times \sum_{k_3=0}^{k_2} \binom{k_2}{k_3} (-1)^{k_3} \frac{(k_1+k_3)!}{\mu^{k_1+k_3+1}} \omega^{k_2-k_3} e^{\frac{-\omega}{c_Q}} \\ & - \sum_{k_1=0}^{2N_R-1} \sum_{k_2=0}^{2N_R-1} a_1 a_2 \frac{\rho^{2(k_1+k_2)} \left(1-\rho^2\right)^{4N_R-2-k_1-k_2}}{k_1! k_2! c_I^{k_1+1} c_Q^{k_2+1}} \sum_{k_3=0}^{k_2} \binom{k_2}{k_3} (-1)^{k_3} \\ & \times \sum_{k_4=0}^{k_1+k_3} \frac{(k_1+k_3)!}{k_4! \mu^{k_1+k_3-k_4+1}} \omega^{k_2-k_3+k_4} e^{\frac{-\omega}{c_I}} \end{aligned} \tag{21}$$

where $\binom{n}{a} \triangleq \frac{n!}{a!(n-a)!}$, $a_1 = \binom{2N_R-1}{2N_R-1-k_1}$, $a_2 = \binom{2N_R-1}{2N_R-1-k_2}$, $c_I = \frac{SNR}{4}\Delta_I^2$, $c_Q = \frac{SNR}{4}\Delta_Q^2$, $\mu = \frac{1}{c_I} - \frac{1}{c_Q}$.

Proof The proof is given in the APPENDIX.

Plugging (21) into (19) yields the average SPEP as follows

$$\begin{aligned}\Pr\left(s\to\hat{s}\right)=&\sum_{k_1=0}^{2N_R-1}\sum_{k_2=0}^{2N_R-1}a_1a_2\times\frac{\rho^{2k_1+2k_2}\left(1-\rho^2\right)^{4N_R-2-k_1-k_2}}{k_1!k_2!c_I^{k_1+1}c_Q^{k_2+1}}\\&\times\sum_{k_3=0}^{k_2}\binom{k_2}{k_3}(-1)^{k_3}\frac{(k_1+k_3)!}{\mu^{k_1+k_3+1}}\int_0^{\infty}\frac{1}{2}erfc\left(\sqrt{\frac{\omega}{2}}\right)e^{\frac{-\omega}{c_Q}}\omega^{k_2-k_3}d\omega\\&-\sum_{k_1=0}^{2N_R-1}\sum_{k_2=0}^{2N_R-1}a_1a_2\times\frac{\rho^{2k_1+2k_2}\left(1-\rho^2\right)^{4N_R-2-k_1-k_2}}{k_1!k_2!c_I^{k_1+1}c_Q^{k_2+1}}\\&\times\sum_{k_3=0}^{k_2}\binom{k_2}{k_3}(-1)^{k_3}\frac{(k_1+k_3)!}{\mu^{k_1+k_3+1}}\\&\times\sum_{k_4=0}^{k_1+k_3}\frac{1}{k_4!\mu^{-k_4}}\int_0^{\infty}\frac{1}{2}erfc\left(\sqrt{\frac{\omega}{2}}\right)e^{\frac{-\omega}{c_I}}\omega^{k_2-k_3+k_4}d\omega\end{aligned}\tag{22}$$

Using Eq. [20 equation (6.286.1)]

$$\int_0^{\infty}\frac{1}{2}erfc\left(\beta\sqrt{x}\right)e^{\alpha^2x}x^{\frac{v-2}{2}}dx=\frac{\Gamma\left(\frac{v+1}{2}\right)}{\sqrt{\pi}v\beta^v}{}_2F_1\left(\frac{v}{2},\frac{v+1}{2};\frac{v}{2}+1;\frac{\alpha^2}{\beta^2}\right)\tag{23}$$

we obtain the average SPEP as

$$\begin{aligned}\Pr\left(s\to\hat{s}\right)=&\sum_{k_1=0}^{2N_R-1}\sum_{k_2=0}^{2N_R-1}a_1a_2\times\frac{\rho^{2k_1+2k_2}\left(1-\rho^2\right)^{4N_R-2-k_1-k_2}}{k_1!k_2!c_I^{k_1+1}c_Q^{k_2+1}}\\&\times\frac{1}{\sqrt{\pi}}\sum_{k_3=0}^{k_2}\binom{k_2}{k_3}(-1)^{k_3}\frac{(k_1+k_3)!}{\mu^{k_1+k_3+1}}\times\frac{2^{k_2-k_3}}{k_2-k_3+1}\Gamma\left(k_2-k_3+\frac{3}{2}\right)\\&\times{}_2F_1\left(k_2-k_3+1,k_2-k_3+\frac{3}{2};k_2-k_3+2;-\frac{2}{c_Q}\right)\\&-\sum_{k_1=0}^{2N_R-1}\sum_{k_2=0}^{2N_R-1}a_1a_2\times\frac{\rho^{2k_1+2k_2}\left(1-\rho^2\right)^{4N_R-2-k_1-k_2}}{k_1!k_2!c_I^{k_1+1}c_Q^{k_2+1}}\\&\times\frac{1}{\sqrt{\pi}}\sum_{k_3=0}^{k_2}\binom{k_2}{k_3}(-1)^{k_3}\frac{(k_1+k_3)!}{\mu^{k_1+k_3+1}}\sum_{k_4=0}^{k_1+k_3}\frac{2^{k_2-k_3+k_4}}{k_4!\mu^{-k_4}\left(k_2-k_3+k_4+1\right)}\\&\times\Gamma\left(k_2-k_3+k_4+\frac{3}{2}\right)\\&\times{}_2F_1\left(k_2-k_3+k_4+1,k_2-k_3+k_4+\frac{3}{2};k_2-k_3+k_4+2;-\frac{2}{c_I}\right)\end{aligned}\tag{24}$$

where ${}_2F_1\left(a,b;c;z\right)$ is Hypergeometric function and $\Gamma(\cdot)$ is Gamma function. We note that the Hypergeometric functions are provided in common mathematical software, such as MATHEMATICAL, MAPLE, etc.

We also emphasize that the average SPEP derivation given in (24) is closed-form for the arbitrary constellation $\mathcal{A}$ and an arbitrary number of receiver antenna N_R. Moreover, from generalized Eq. (24), we easily obtain average SPEP on two special cases: the quasi-static fading channel ($\rho = 1$) and the fast fading channel ($\rho = 0$).

Special case 1: For $\rho = 1$, quasi-static fading channel

$$\begin{aligned}\Pr\left(s \to \hat{s}\right) = &\frac{1}{\left[(2N_R-1)!\right]^2 \left(c_I c_Q\right)^{2N_R}} \frac{1}{\sqrt{\pi}} \sum_{k_3=0}^{2N_R-1} \binom{k_2}{k_3} (-1)^{k_3} \frac{(2N_R-1+k_3)!}{\mu^{2N_R+k_3}} \\ &\times \frac{2^{2N_R-1-k_3}}{2N_R-k_3} \times \Gamma\left(2N_R-k_3+\frac{1}{2}\right) \\ &\times {}_2F_1\left(2N_R-k_3, 2N_R-k_3+\frac{1}{2}; 2N_R-k_3+1; -\frac{2}{c_Q}\right) \\ &- \frac{1}{\left[(2N_R-1)!\right]^2 \left(c_I c_Q\right)^{2N_R}} \\ &\times \frac{1}{\sqrt{\pi}} \sum_{k_3=0}^{2N_R-1} \binom{2N_R-1}{k_3} (-1)^{k_3} \frac{(2N_R-1+k_3)!}{\mu^{2N_R+k_3}} \\ &\times \sum_{k_4=0}^{2N_R-1+k_3} \frac{2^{2N_R-1-k_3+k_4}}{k_4! \mu^{-k_4} \left(2N_R-k_3+k_4\right)} \Gamma\left(2N_R-k_3+k_4+\frac{1}{2}\right) \\ &\times {}_2F_1\left(2N_R-k_3+k_4, 2N_R-k_3+k_4+\frac{1}{2}; 2N_R-k_3+k_4+1; -\frac{2}{c_I}\right)\end{aligned} \tag{25}$$

Special case 2: For $\rho = 0$, fast fading channel

$$\Pr\left(s \to \hat{s}\right) = \frac{1}{\sqrt{\pi} c_I c_Q \mu} \Gamma\left(\frac{3}{2}\right) \times \left[{}_2F_1\left(1, \frac{3}{2}; 2; -\frac{2}{c_Q}\right) - {}_2F_1\left(1, \frac{3}{2}; 2; -\frac{2}{c_I}\right)\right] \tag{26}$$

From Eq. (26), we conclude that when the channel is fast fading (channel gains change independently from symbol to symbol), therefore increasing the number of receiver antennas does not come with any performance improvement for the ZF decoder. This conclusion is confirmed by simulation results in Figs. 1 and 2.

From the average SPEP expression (24), we can find the union bound (UB) on SER of CIOD codes over time-selective fading channel with the ZF decoder and rotated constellation $\mathcal{A}e^{\mathrm{j}\theta}$ as

$$P_{UB} = \frac{1}{|\mathcal{A}|} \sum_{s \in \mathcal{A}\theta e^{j\theta}} \sum_{s \neq \hat{s}} \Pr\left(s \to \hat{s}\right) \tag{27}$$

Although the above performance analysis process is presented for the CIOD code with $N_R = 4$ (i.e., $\boldsymbol{S}_4$), the performance analysis process can be directly applied for CIOD code with $N_T = 3$ (i.e., $\boldsymbol{S}_3$) over time-selective fading channels. The calculation details are omitted and we only provide the final result for brevity. The average SPEP of CIOD code with $N_T = 3$ is given in Eq. (28).

$$
\begin{aligned}
\Pr\left(s \to \hat{s}\right) &= \sum_{k_1=0}^{2N_R-1} \sum_{k_2=0}^{N_R-1} a_1 \bar{a}_2 \times \frac{\rho^{2k_1+2k_2}\left(1-\rho^2\right)^{3N_R-2-k_1-k_2}}{k_1!k_2!\bar{c}_I^{k_1+1}\bar{c}_Q^{k_2+1}} \\
&\times \frac{1}{\sqrt{\pi}} \sum_{k_3=0}^{k_2} \binom{k_2}{k_3} (-1)^{k_3} \frac{(k_1+k_3)!}{\bar{\mu}^{k_1+k_3+1}} \times \frac{2^{k_2-k_3}}{k_2-k_3+1} \Gamma\left(k_2-k_3+\frac{3}{2}\right) \\
&\times {}_2F_1\left(k_2-k_3+1, k_2-k_3+\frac{3}{2}; k_2-k_3+2; -\frac{2}{\bar{c}_Q}\right) \\
&- \sum_{k_1=0}^{2N_R-1} \sum_{k_2=0}^{N_R-1} a_1 \bar{a}_2 \times \frac{\rho^{2k_1+2k_2}\left(1-\rho^2\right)^{3N_R-2-k_1-k_2}}{k_1!k_2!\bar{c}_I^{k_1+1}\bar{c}_Q^{k_2+1}} \\
&\times \frac{1}{\sqrt{\pi}} \sum_{k_3=0}^{k_2} \binom{k_2}{k_3} (-1)^{k_3} \frac{(k_1+k_3)!}{\bar{\mu}^{k_1+k_3+1}} \sum_{k_4=0}^{k_1+k_3} \frac{2^{k_2-k_3+k_4}}{k_4!\bar{\mu}^{-k_4}\left(k_2-k_3+k_4+1\right)} \\
&\times \Gamma\left(k_2-k_3+k_4+\frac{3}{2}\right) \\
&\times {}_2F_1\left(k_2-k_3+k_4+1, k_2-k_3+k_4+\frac{3}{2}; k_2-k_3+k_4+2; -\frac{2}{\bar{c}_I}\right)
\end{aligned} \tag{28}
$$

where $\bar{a}_2 = \binom{N_R-1}{N_R-1-k_2}$, $\bar{\Delta}_I^2 = \frac{|u_I-\hat{u}_I|^2}{E_s/2}$, $\bar{c}_I = \frac{SNR}{3}\bar{\Delta}_I^2$, $\bar{\Delta}_Q^2 = \frac{|u_Q-\hat{u}_Q|^2}{E_s}$, $\bar{c}_Q = \frac{SNR}{3}\bar{\Delta}_Q^2$, and $\bar{\mu} = \frac{1}{\bar{c}_I} - \frac{1}{\bar{c}_Q}$.

4 Simulation Results

In order to check the accuracy of the theoretical error analysis, we have carried out Monte-Carlo simulations for ZF detector (17) with channel model (3) and then compared them with the theoretical analysis. Two typical Doppler spreads in this section are $f_d T_s = 0.03$ ($\rho = 0.9911$) and $f_d T_s = 0.0687$ ($\rho = 0.954$). Two typical Doppler spreads correspond to a 1.9 GHz personal communications services (PCS) system, in which the symbol rate is 6.4 kBd and the speed of the mobile is 112 km/h and 250 km/h. Two extreme cases: the quasi-static channel ($\rho = 1$) and the fast fading channel ($\rho = 0$) are also considered. The SER versus SNR curves are presented in Fig. 1 for various antenna configurations (N_T, N_R) and 4QAM constellation with rotation phase $\theta = 31.7175$ degrees.

Figures 1 and 2 present comparisons between simulation results and theoretical analysis for $N_\mathrm{T} = 4$ and $N_\mathrm{R} = 1, 2$ receive antennas. The exact SER curves are obtained by Monte-Carlo simulations over 10^8 independent channel realizations and the curves for the union bound on the SER are performed by Eq. (27). These figures show our upper bound is very tight for any value of ρ and arbitrary number of receiver antenna at high SNR values. This demonstrates that theoretical UB on the SER is exact and coincides (within 0.05 dB) with the simulated SER for various fading parameters and different antenna configurations. Similar results can be found for cases $N_T = 2$ and 3; details are omitted for brevity.

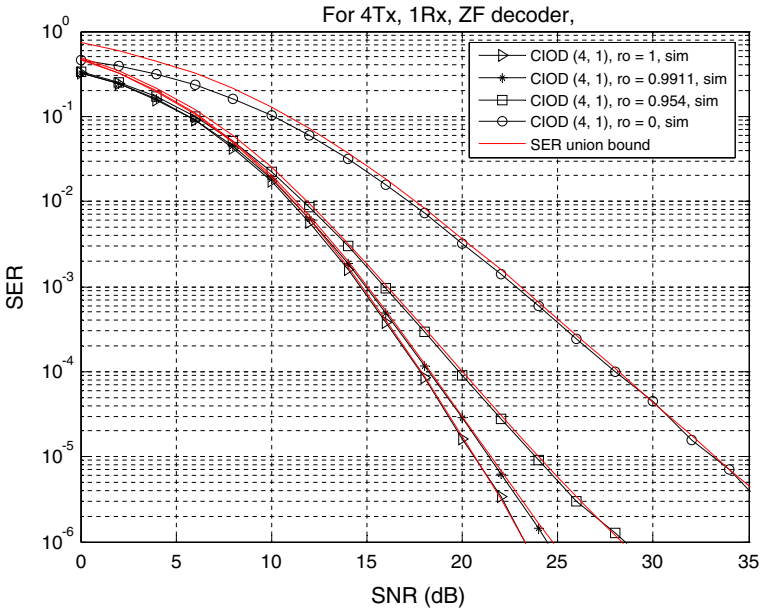

Fig. 1 Comparison of the union bound of SER and simulated SER of CIOD code S_4 for different correlated factors with the ZF decoder and one receive antenna. In this figure, the correlation factor ρ is denoted as ro

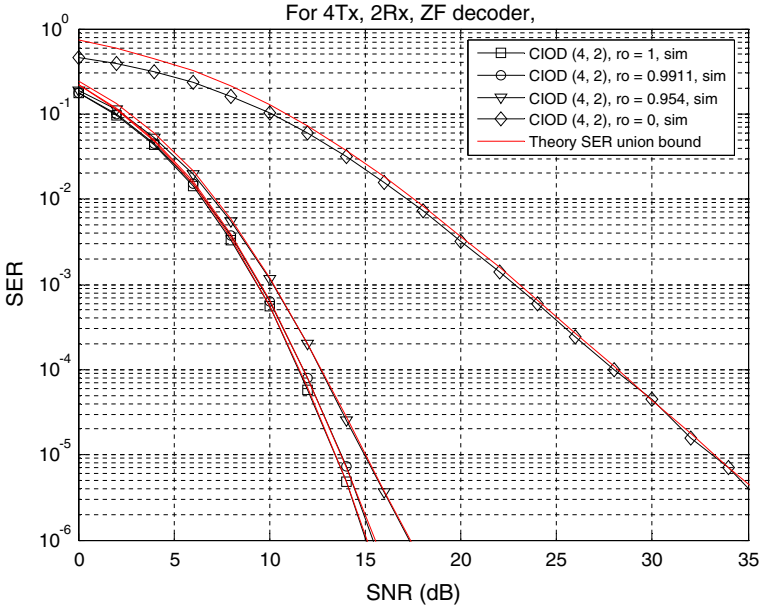

Fig. 2 Comparison of the union bound of SER and simulated SER of CIOD code S_4 for different correlated factors with the ZF decoder and two receive antenna. In this figure, the correlation factor ρ is denoted as ro

5 Conclusions

A closed-form expression of SPEP for CIOD codes with ZF decoder over time-selective fading channel is derived. Based on the exact expression of SPEP, a union bound on the SER of CIOD codes is also established. The accuracy of the union bound has been confirmed by comparison with the SER curves obtained from Monte-Carlo simulation. A decisive agreement between theoretical analysis and simulation result demonstrated that our union bound can be used to accurately predict the performance of CIOD codes over time-selective fading channels. Moreover, our performance analysis is not restricted by modulation types, so it can be applied to analyze and find optimum constellation for CIOD codes.

Appendix

To proof Theorem 1, we firstly introduce Lemma 1 as follow:

Lemma 1 *Let* $X_1 = \frac{|g_1|^2}{\lambda_1}\frac{SNR}{4}\Delta_I^2 = \frac{|g_1|^2}{\lambda_1}c_I$ *and* $X_2 = \frac{|g_2|^2}{\lambda_3}\frac{SNR}{4}\Delta_Q^2 = \frac{|g_2|^2}{\lambda_3}c_Q$ *then* X_1 *and* X_2 *are independent random variables whose probability density functions (PDFs) respectively are*

$$p_{X_1}(x) = \sum_{k=0}^{2N_R-1}\binom{2N_R-1}{2N_R-1-k}\frac{\rho^{2k}\left(1-\rho^2\right)^{2N-1-k}}{k!c_I^{k+1}}x^k\exp\left(\frac{-x}{c_I}\right) \tag{29}$$

$$p_{X_2}(y) = \sum_{k=0}^{2N_R-1}\binom{2N_R-1}{2N_R-1-k}\frac{\rho^{2k}\left(1-\rho^2\right)^{2N-1-k}}{k!c_Q^{k+1}}y^k\exp\left(\frac{-y}{c_Q}\right) \tag{30}$$

Proof The proof of Eqs. (29) and (30) is the same, so we consider the proof of Eq. (29). Let us introduce the random variables ξ_{1k} and ξ_{2k}, $k = 1, ..., N_R$

$$\xi_{1k} = \frac{h_{1k}(1) - \rho h_{1k}(2)}{\sqrt{1-\rho^2}};\ \xi_{2k} = \frac{h_{2k}(2) - \rho h_{2k}(1)}{\sqrt{1-\rho^2}} \tag{31}$$

where we assume $\rho^2 < 1$. By construction, ξ_{1k} and ξ_{2k} are independent and identically distributed with the same pdf as $h_{1k}(2)$ and $h_{2k}(1)$; furthermore, ξ_{1k} is independent of $h_{1k}(2)$, ξ_{1k} and is independent of $h_{2k}(1)$. Plugging (31) into X_1 leads to

$$X_1 = \left|\rho\sqrt{\lambda_1} + \sqrt{1-\rho^2}\frac{\sum_{k=1}^{N_R}\left(h_{1k}^*(2)\xi_{1k} + h_{2k}(1)\xi_{2k}^*\right)}{\sqrt{\lambda_1}}\right|^2 c_I \tag{32}$$

To simplify this expression further, observe that the fraction in (32) can be expressed as an inner product

$$z_1 + \mathrm{j}z_2 = \frac{\sum_{k=1}^{N_R}\left(h_{1k}^*(2)\xi_{1k} + h_{2k}(1)\xi_{2k}^*\right)}{\sqrt{\lambda_1}} = \left\langle\frac{\boldsymbol{h}}{\|\boldsymbol{h}\|}, \boldsymbol{e}\right\rangle \tag{33}$$

where z_1, z_2 are real variables, $\boldsymbol{h} = \left[h_{11}(2), h_{21}^*(1), \ldots, h_{1N_R}(2), h_{2N_R}^*(1)\right]^{\mathrm{T}}$ and $\boldsymbol{e} = \left[\xi_{11}^*, \xi_{21}, \ldots, \xi_{1N_R}^*, \xi_{2N_R}\right]^{\mathrm{T}}$. Since $\boldsymbol{e}$ is symmetric, the distribution of $z_1 + \mathrm{j}z_2$ reduces to the distribution of $h_{1k}(1)$, independent of $\boldsymbol{h}$ (and, thus, also independent of $\|\boldsymbol{h}\|$). Thus, (33)

simplifies to

$$X_1 = \left|\rho\sqrt{\lambda_1} + \sqrt{1-\rho^2}\,(z_1 + \mathrm{j}z_2)\right|^2 c_I \tag{34}$$

$$X_1 = (A + Z_1)^2 + Z_2^2 \tag{35}$$

where $A = \sqrt{\lambda_1 \rho^2 c_I}$ and $Z_i = \sqrt{\left(1-\rho^2\right) c_I}\, z_i$, $i = 1, 2$. Therefore, given A, X_1 has a noncentral chi-square distribution with two degrees of freedom, and PDF

$$p_{X_1|A}\,(x\,|a\,) = \frac{1}{\left(1-\rho^2\right) c_I} \exp\left(-\frac{x + a^2}{\left(1-\rho^2\right) c_I}\right) J_0\left(\frac{2\mathrm{j}a}{\left(1-\rho^2\right) c_I}\sqrt{x}\right) \tag{36}$$

where $J_0(\cdot)$ is the zeroth-order Bessel function of the first kind, and $\mathrm{j} = \sqrt{-1}$.

However, $A = \sqrt{\lambda_1 \rho^2 c_I}$ is Rayleigh distributed with $2N_R$ degrees of freedom with PDF

$$p_A(a) = \frac{2}{\rho^{4N_R} c_I^{2N_R} \Gamma\left(2N_R\right)} a^{4N_R - 1} \exp\left(-\frac{a^2}{\rho^2 c_I}\right) \tag{37}$$

Integrating the product of (36) and (37) over the variable from 0 to ∞ leads to the following PDF for x as

$$p_{X_1}(x) = \int_0^\infty p_{X_1|A}\,(x\,|a\,) p_A(a) da \tag{38}$$

$$p_{X_1}(x) = \frac{2}{\left(1-\rho^2\right) \rho^{4N_R} c_I^{2N_R+1} \Gamma\left(2N_R\right)} \exp\left(-\frac{x}{\left(1-\rho^2\right) c_I}\right) \times \int_0^\infty a^{4N_R-1} \exp\left(-\frac{a^2}{\left(1-\rho^2\right) \rho^2 c_I}\right) J_0\left(\frac{2\mathrm{j}\sqrt{x}}{\left(1-\rho^2\right) c_I} a\right) da \tag{39}$$

From (40), by using [17, equation(6.631.1)] we obtain

$$p_{X_1}(x) = \frac{\left(1-\rho^2\right)^{2N_R-1}}{c_I} \exp\left(-\frac{x}{\left(1-\rho^2\right) c_I}\right) {}_1F_1\left(2N_R, 1; \frac{\rho^2}{\left(1-\rho^2\right) c_I} x\right) \tag{40}$$

where ${}_1F_1\,(\alpha, \beta; z)$ is Kummer confluent hypergeometric function [17]. By applying equations given in [18,19] we have

$${}_1F_1\left(2N_R, 1; \frac{\rho^2}{\left(1-\rho^2\right) c_I} x\right) = \exp\left(\frac{\rho^2 x}{\left(1-\rho^2\right) c_I}\right) \times \sum_{k=0}^{2N_R-1} \binom{2N_R - 1}{2N_R - 1 - k} \frac{\rho^{2k}}{k!\left(1-\rho^2\right)^k c_I^k} x^k \tag{41}$$

Plugging (41) into (40) we obtain

$$p_{X_1}(x) = \sum_{k=0}^{2N_R-1} \binom{2N_R - 1}{2N_R - 1 - k} \frac{\rho^{2k}\left(1-\rho^2\right)^{2N-1-k}}{k! c_I^{k+1}} x^k \exp\left(\frac{-x}{c_I}\right) \tag{42}$$

The proof of Eq. (30) is similar. The Lemma 1 is demonstrated completely.

Remark 1 It is very interesting that although the calculation process from (31) to (42) is performed under the assumption $\rho^2 < 1$, the final result (42) is general and can apply to any value of ρ (which includes $\rho^2 = 1$). The proof of this observation is not difficult, so it is omitted here for brevity.

Next, we use Lemma 1 to demonstrate Theorem 1. Since $X_1,\ X_2$ are independent random variables, thus the PDF of ω, which $\omega = X_1 + X_2$, is expressed by

$$p_W(\omega) = \int_0^{\omega} p_{X_1}(x) p_{X_2}(\omega - x)\, dx \tag{43}$$

Plugging Eqs. (29) and (30) into Eq. (43), we obtain

$$p_W(\omega) = \sum_{k_1=0}^{2N_R-1} \sum_{k_2=0}^{2N_R-1} a_1 a_2 \frac{\rho^{2k_1+2k_2} \left(1-\rho^2\right)^{4N_R-2-k_1-k_2}}{k_1! k_2! c_I^{k_1+1} c_Q^{k_2+1}} e^{\frac{-\omega}{c_Q}} \int_0^{\omega} e^{-\mu x} x^{k_1} (\omega - x)^{k_2}\, dx \tag{44}$$

where $\binom{n}{a} \triangleq \frac{n!}{a!(n-a)!}$, $a_1 = \binom{2N_R-1}{2N_R-1-k_1}$, $a_2 = \binom{2N_R-1}{2N_R-1-k_2}$, and $\mu = \frac{1}{c_I} - \frac{1}{c_Q}$.

By applying Newton's binomial

$$x^{k_1} (\omega - x)^{k_2} = \sum_{k_3=0}^{k_2} \binom{k_2}{k_3} (-1)^{k_3} \omega^{k_2-k_3} x^{k_1+k_3} \tag{45}$$

we obtain

$$p_W(\omega) = \sum_{k_1=0}^{2N_R-1} \sum_{k_2=0}^{2N_R-1} a_1 a_2 \frac{\rho^{2k_1+2k_2} \left(1-\rho^2\right)^{4N_R-2-k_1-k_2}}{k_1! k_2! c_I^{k_1+1} c_Q^{k_2+1}} e^{\frac{-\omega}{c_Q}} \sum_{k_3=0}^{k_2} \binom{k_2}{k_3} (-1)^{k_3} \omega^{k_2-k_3} \times \int_0^{\omega} e^{-\mu x} x^{k_1+k_3} dx \tag{46}$$

Then, using Eq. [17, equation (3.351.1)],

$$\int_0^{\alpha} x^n e^{-\mu x} dx = \frac{n!}{\mu^{n+1}} - e^{-\mu\alpha} \sum_{k=0}^{n} \frac{n!}{k!} \frac{\alpha^k}{\mu^{n-k+1}} \tag{47}$$

we obtain

$$p_W(\omega) = \sum_{k_1=0}^{2N_R-1} \sum_{k_2=0}^{2N_R-1} a_1 a_2 \frac{\rho^{2(k_1+k_2)} \left(1-\rho^2\right)^{4N_R-2-k_1-k_2}}{k_1! k_2! c_I^{k_1+1} c_Q^{k_2+1}} \times \sum_{k_3=0}^{k_2} \binom{k_2}{k_3} (-1)^{k_3} \frac{(k_1+k_3)!}{\mu^{k_1+k_3+1}} \omega^{k_2-k_3} e^{\frac{-\omega}{c_Q}}$$

$$- \sum_{k_1=0}^{2N_R-1} \sum_{k_2=0}^{2N_R-1} a_1 a_2 \frac{\rho^{2(k_1+k_2)} \left(1-\rho^2\right)^{4N_R-2-k_1-k_2}}{k_1! k_2! c_I^{k_1+1} c_Q^{k_2+1}} \sum_{k_3=0}^{k_2} \binom{k_2}{k_3} (-1)^{k_3}$$
$$\times \sum_{k_4=0}^{k_1+k_3} \frac{(k_1+k_3)!}{k_4! \mu^{k_1+k_3-k_4+1}} \omega^{k_2-k_3+k_4} e^{\frac{-\omega}{c_I}} \tag{48}$$

The Theorem 1 is demonstrated completely.

References

1. Tarokh, V., Seshadri, N., & Calderbank, A. R. (1998). Space-time codes for high data rate wireless communication: Performance criterion and code construction. *IEEE Transactions on Information Theory*, *44*(2), 744–765.
2. Alamouti, S. M. (1998). A simple transmit diversity technique for wireless communications. *IEEE Journal of Selected Areas in Communications*, *16*(8), 1451–1458.
3. Tarokh, V., Jafarkhani, H., & Calderbank, A. R. (1999). Space-time block codes from orthogonal designs. *IEEE Transactions on Information Theory*, *45*(5), 1456–1467.
4. Jafarkhani, H. (2001). A quasi-orthogonal space-time block code. *IEEE Transactions on Communications*, *49*(1), 1–4.
5. Tirkkonen, O., Boariu, A., & Hottinen, A. (2000). Minimal non-orthogonality rate 1 space-time block code for 3+ Tx antennas. In *Proceedings of IEEE International Symposium on Spread-Spectrum Techniques and Applications (ISSSTA'00)*, (pp. 429–432). New Jersey, USA.
6. Papadias, C. B., & Foschini, G. J. (2003). Capacity-approaching space-time codes for systems employing four transmitter antennas. *IEEE Transactions on Information Theory*, *49*(3), 726–732.
7. Sharma, N., & Papadias, C. B. (2003). Improved quasi-orthogonal codes through constellation rotation. *IEEE Transactions on Communications*, *51*(3), 332–335.
8. Su, W., & Xia, X.-G. (2004). Signal constellations for quasi-orthogonal space-time block codes with full diversity. *IEEE Transactions on Information Theory*, *50*(10), 2331–2347.
9. Khan, M.Z.A., & Rajan, B.S. (2002). Space-time block codes from co-ordinate interleaved orthogonal designs. In *Proceedings of the IEEE International Symposium on Information (ISIT)*, Switzerland: Lausanne.
10. Khan, Z. A., & Rajan, B. S. (2006). Single-symbol maximum likelihood decodable linear STBCs. *IEEE Transactions on Information Theory*, *52*(5), 2062–2091.
11. Đào, D. N., & Tellambura, C. (2008). Decoding, performance analysis, and optimal signal designs for coordinate interleaved orthogonal designs. *IEEE Transactions on Wireless Communications*, *7*(1), 48–53.
12. Lee, H. J., Andrews, J. G., Heath, R. W., & Powers, E. J. (2009). The performance of space–time block codes from coordinate interleaved orthogonal designs over Nakagami-*m* Fading channels. *IEEE Transactions on Wireless Communications*, *57*(3), 653–664.
13. Lee, Hoojin, Andrews, Jeffrey G., & Edward, J. (2008). Powers: Full-rate STBCs from coordinate interleaved orthogonal designs in time-selective fading channels. *IEICE Transactions*, *91–B*(4), 1185–1189.
14. Jakes, W. C. (1974). *Microwave mobile communication*. New Jersey: Wiley.
15. Tran, T. A., & Sesay, A. B. (2004). A generalized simplified ML decoder of orthogonal space–time block code for wireless communications over time-selective fading channels. *IEEE Transactions on Wireless Communications*, *3*(3), 855–864.
16. Vielmon, A., Li, Y(. G)., & Barry, J. R. (2004). Performance of Alamouti transmit diversity over time-varying Rayleigh-Fading channels. *IEEE Transactions on Wireless Communications*, *3*(5), 1369–1373.
17. Gradshteyn, I. S., & Ryzhik, I. M. (2007). *Table of integrals, series, and products*. Massachusetts: Academic Press.
18. http://functions.wolfram.com/HypergeometricFunctions/Hypergeometric1F1/03/01/02/0011. Accessed May (2013)
19. http://functions.wolfram.com/HypergeometricFunctions/LaguerreL3General/06/01/03/01/02/0001. Accessed May (2013)

Van-Bien Pham was born in Hanoi, Vietnam in November 1978. He received his B.S. and M.S. degrees in electronic engineering from Le Quy Don Technical University, Hanoi, Vietnam in 2002 and 2005, and his Ph.D. degree in information and communication engineering from Nanjing University of Science and Technology, Nanjing, China in 2012. Now, he is a lecturer at Faculty of Radio-Electronics, Le Quy Don Technical University, Hanoi, Vietnam. His research interests include MIMO wireless communication, cognitive radio, network coding, cooperative communication and space-time coding.